Journal Name

ARTICLE

Aggregation-induced scaffolding: Photoscissable helical polysilane generates circularly polarized luminescent polyfluorene

Nor Azura Abdul Rahim[a,b] and Michiya Fujiki[a,*]

made Received 00th January 20xx,
Accepted 00th January 20xx

DOI: 10.1039/x0xx00000x

www.rsc.org/

An enantiopair of rigid rod-like helical polysilanes (**PSi-*S***and **PSi-*R***) as a photoscissible scaffold enabled the production of circularly polarised luminescence (CPL)- and circular dichroism (CD)-active di-*n*-octylpolyfluorene (**PF8**) aggregates associated with complete removal by **PSi**-selective photoscissoring at 313 nm. **PF8** revealed a considerably high dissymmetry factor (g_{CPL}) of (2−5) × 10^{-3} at 435 nm due to chiral β-phase of **PF8** after the 313-nm irradiation.

1. Introduction

The origin of biomolecular handedness on Earth is one of the greatest mysteries among geochemists and chiral scientists.[1] A possible answer to this unresolved question has been lost due to the complete loss of fossil records at the molecular level. Nevertheless, one can assume that a trace amount of chiral molecular species may act as a scaffold leading to the L-D preferences in the primordial Era[1f–1i] even though all molecular evidence has completely disappeared as a consequence of chemical and photochemical scissoring reactions.

However, in materials science, several biological and artificial helix scaffolds with adaptability towards other achiral/chiral molecular, oligomeric and polymeric resources because of rotational freedom along the C–C, C–O and C–N single bonds can be utilised to build-up helical architectures with desired functions.[2,3] A representative cryoexample is triple-helix collagens in tissue engineering.[2a] Other polymeric and oligomeric materials, such as synthetic polymers, DNA, oligopeptides, polysaccharides, carbon nanotubes and aromatic foldamers, are candidates for chiroptical and other functional scaffolding.[2b-2i,3] However, completely removing these scaffolds from the resulting helically hybridised skeletons while maintaining the designed functions is a difficult task because the C–C single-bond-based scaffolding ability is both chemically and photochemically strong due to the sum of the weak intermolecular interactions.

Certain organic gelators, that enable to generate helical inorganic motifs by sol-gel process with alkoxysilanes and tetraethoxysilane, might be scaffolding because most of organic moieties are removable by calcination and carbonation at high temperatures (500–900°C).[3a–3c] Alternatively, macromolecular helicity induced by chiral amines can be kept by replacing with achiral amines and amino alcohols at room temeperature.[2l] The starting chiral amines sources are regarded as scaffolding. More recently, Liu *et al*. demonstrated that an amphiphilic L- or D-glutamide gelator generates circularly polarised luminescence (CPL)- and circular dichroism (CD)-active π-conjugated polyfluorene analogs during gelation with the aid of hydrogen bonds and hydrophobic forces, followed by removal of the glutamide via washing with methanol at room temeperature.[3d] Also, helicity of cationic molecular assemblies in water inverts kinetically by changing molar ratio between D- and L-tartrates. However, the tartrate did not act as scaffolding because the induced helicity completely disappeared after removal of the tartrate.[3e]

Shinkai *et al* demonstrated several helicity transfer experiments in water-DMSO cosolvent from non-charged helical polysaccharide (schizophyllan and curdlan) to CD-/CPL-silent cationic charge polythiophene with stoichiometric 1-to-1 ratio and CD-/CPL-silent anionic charge poly(fluorene-*alt*-*m*-phenylene) with non-stoichiometric 13-to-8 ratio as repeating units.[2h-2k] This macromolecule-to-macromolecule complexation can instantly form the corresponding CD- and CPL-active π-conjugated polymers. Alternatively, cationic charge curdlan forms a complex with non-charged permethyloligosilane and single-walled carbon nanotubes.[2k]

Herein, we questioned whether these approaches are applicable to complexation between two non-charged artificial polymers without specific intermolecular interactions. Actually, we reported several aggregation-induced CPL- and CD-active π- and σ-conjugated polymers induced by molecular chirality transfer of non-charged limonene, α-pinene and alcohols.[4] In these cases, all of the starting polymers, which are non-charged and devoid of stereogenic centres in their main chain and side chains, are CD-silent dynamic helical polymers because of their substantial rotational freedom, which has a low barrier height

[a] *Graduate School of Materials Science, Nara Institute of Science and Technology, 8916-5 Takayama, Ikoma, Nara 630-0192, Japan. E-mail: fujikim@ms.naist.jp*
[b] *School of Materials Engineering, Universiti Malaysia Perlis, 02600, Arau, Perlis, Malaysia. E-mail: nor.azura.ms5@ms.naist.jp, norazura@unimap.edu.my*

† Electronic Supplementary Information (ESI) available: Experimental sections, materials synthesis and characterisation, chiral GC and GPC-VISCO data, CPL/PL spectra, cryo-TEM images and AFM images. See DOI: 10.1039/x0xx00000x

on the order of 5–10 kJ mol^{-1}. The optically active solvents are regarded as volatile chiral fluidic scaffolds that are removable at ambient temperatures.[4a] Multiple chiral intermolecular CH/π, π/π and London dispersion interactions are assumed to be responsible for the emergence of the aggregation-induced chiroptical polymers.[4]

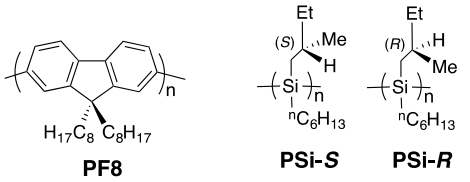

Fig 1. Chemical structures of **PF8**, **PSi-*S*** and **PSi-*R***.

From the perspective of the chiral scaffold hypothesis in the Primordial Era in the absence of circularly polarised UV-vis light source on Earth and interstellar Universe, we showcased the first photochemically controlled scaffolding experiment using hetero-aggregates constructed from non-charged helical dialkylpolysilane (**PSi**) and non-charged non-helical poly(9,9-di-*n*-octylfluorene) (**PF8**) upon irradiation with unpolarised UV light at 313 nm. This approach allows for successful CPL- and CD-active **PF8** aggregates and complete removal of helical **PSi**. An enantiopair consisting of rigid rod-like poly(*n*-hexyl-(*S*)-2-methylbutylsilane) (**PSi-*S***) and poly(*n*-hexyl-(*R*)-2-methylbutylsilane) (**PSi-*R***) was chosen as a *photoscissible h*elix scaffolding. Notably, the Si–Si bond in dialkylpolysilanes homolytically ruptures upon prolonged irradiation at wavelengths corresponding to the Siσ–Siσ□ absorption bands (i.e., approximately 300–320 nm), yielding silyl radicals and lower-molecular-weight organosilane species.[5] Therefore, **PSi-*R*** and **PSi-*S*** are the best candidate helical polymers for achieving a *photoscissoring* helix scaffolding system, and non-helical **PF8**, which is photochemically robust, efficiently produces blue-coloured photoluminescence.[6] The noticeable difference in the photoscissoring ability of **PSi-*R*** (and **PSi-*S***) and **PF8** is the key idea underlying the design of the current helix scaffolding systems.

The helix scaffolding protocol involves two major steps. The first step is to concurrently aggregate **PF8** and helical **PSi-*R*** (and **PSi-*S***) in the desired molar ratio by adding their common poor solvent (methanol) to a common toluene solution of **PF8** and **PSi** under their optimal volume fraction.

This catalyst-free process allows for the instantaneous (typically, 5–10 s) emergence of hetero-aggregates composed of CPL- and CD-active **PF8** with CD-active **PSi-*R*** (and **PF8** with **PSi-*S***) at ambient temperature (Fig. 1). Hetero-aggregates with **PSi-*R*** (and **PSi-*S***) restrict the rotational freedom in **PF8**, which is typical of the aggregation-induced emission effect.[7] Multiple intermolecular CH/π, π/π and van der Waals interactions are responsible for the optical activity of **PF8**.[4] The second involves complete removal of **PSi-*R*** (or **PSi-*S***) by a **PSi**-selective photochemical Si–Si scissoring reaction[5b] to yield persistently CPL- and CD-active **PF8**.

We confirmed all of these processes before and after removal of the scaffolds using CD/UV/CPL/photoluminescence (PL) spectroscopy, transmission electron microscopy (TEM), atomic force microscopy (AFM), dynamic light scattering (DLS), PL decay dynamics and partial confirmation by the naked eye.

2. Experimental Section

2.1 Materials

2.1.1. Preparation of PSi

Poly(*n*-hexyl-(*S*)-2-methylbutylsilane) (**PSi-*S***) and poly(*n*-hexyl-(*R*)-2-methylbutylsilane) (**PSi-*R***) were prepared and characterised according to the provided electronic supporting information (ESI).

2.1.2. Fractionation of PF8

The achiral **PF8**, which was obtained from Sigma-Aldrich Japan (Tokyo, Japan), with a PDI of 3.6 was fractionated by the addition of a poor solvent to a chloroform solution containing the **PF8**. In the fractionation process, **PF8** was first dissolved in chloroform (Wako, special grade) followed by the gradual addition of isopropanol (IPA) and stirring until the aggregate precipitated in the stock solution. The polymer was then filtered with a Whatman® PTFE 1.0 μm membrane filter. The remaining **PF8** on the filler was collected and dried in a vacuum oven overnight. Similar fractionation processes were repeated with higher-polarity solvents (i.e., ethanol and methanol) and, ultimately, distilled water. **PF8** with M_n of 78,400 with 1.8 PDI was chosen for this study.

2.1.3. Hetero-aggregation of fractionated PF8 and PSi

Spectroscopic-grade toluene and chloroform (Dojindo, Kumamoto, Japan) as good solvents and methanol (Dojindo) as a poor solvent were added to produce an optically active hetero-aggregate in a 10 mm synthetic quartz (SQ)-grade quartz cuvette. The optimized volume ratio was 1:1, with the total volume content of mixed toluene and methanol being fixed at 3.0 mL. The molar ratio of the polymers in dissolved toluene was tuned according to the experimental requirements. The dissolved **PF8** was added to the cuvette, followed by the rapid addition of fractionated **PSi-*S*** (M_n = 75,800, *PDI* = 1.3) or **PSi-*R*** (M_n = 73,900, *PDI* = 1.4) to produce a well-mixed complex, and methanol was slowly added. Simultaneously, CD-UV-Vis and CPL-PL spectroscopic data were collected within several minutes after completion of the hetero-aggregation process.

2.2. Characterisation

2.2.1 Chiroptical analysis[8,9]

The magnitude of CD in the ground state was calculated as g_{CD} = 2 × ($\varepsilon_L - \varepsilon_R$) / ($\varepsilon_L + \varepsilon_R$), where ε_L and ε_R are the extinction coefficients for left and right circularly polarised light, respectively. Parameter g_{CD} was obtained as follows: $\Delta\varepsilon/\varepsilon$ = [ellipticity/32,980]/ absorbance at the CD extremum of the hetero-aggregates. The degree of circular polarisation in the photoexcited state was defined as g_{CPL} = 2 × (□$_L$ − □$_R$) / (□$_L$ + □$_R$) at the CPL extremum of the hetero-aggregates, where □$_L$ and □$_R$ are the output signals for left and right circularly polarized emission, respectively.

2.2.2 Refractive index of cosolvents

The refractive index (n_D) value was evaluated by the equation $n_{D.ave} = x\ n_{D(MeOH)} + (1 - x)\ n_{D(Toluene)}$, where x is the volume

fraction of MeOH in the cosolvent. The n_D values of pure MeOH and toluene were used for this evaluation.

2.2.3 Number-average degree of polymerization

The main chain lengths of **PF8**, **PSi-*S*** and **PSi-*R*** were evaluated by the product of their monomer unit lengths and number-average degree of polymerization $DP_n = M_n/M_0$, where M_n and M_0 are the number-average of molecular weight and the molecular weight of the monomer unit.

2.3 Instrumentation

The CD/UV-Vis spectra of the aggregate were recorded using a JASCO (Tokyo, Japan) J-820 spectropolarimeter with a Peltier-controlled equipment to control solution temperature. A scanning rate of 100 nm min^{-1}, a bandwidth of 2 nm and a response time of 1 s at 20 °C were used to simultaneously obtain the CD and UV-Vis spectra. The CPL/PL spectra were recorded at 20 °C on a JASCO CPL-200 spectrofluoropolarimeter with a Peltier-controlled equipment. A path length of 10 mm, scanning rate of 100 nm min^{-1}, bandwidth for excitation of 10 nm, bandwidth for monitoring of 10 nm, response time of photomultiplier tube of 2 s and single accumulation were applied during the measurements.

The dichlorosilane monomers and their starting source materials were characterised by ^{13}C- (75.43 MHz) and ^{29}Si- (59.59 MHz) NMR spectra in $CDCl_3$ at 30 °C with a Varian Unity 300 MHz NMR spectrometer (now, as a member of Agilent Technologies (Palo Alto, California)) with tetramethylsilane as the internal standard. The optical rotation at the Na-D line was measured with a JASCO DIP-370 polarimeter using a synthetic quartz (SQ) cuvette with a path length of 10 mm at room temperature (24 °C). The weight-average molecular weight (M_w), M_n and polydispersity index ($PDI = M_w/M_n$) were evaluated by gel-permeation chromatography (GPC) of a Shimadzu (Kyoto, Japan) A10 chromatogaph with a Shodex KF-806M column and a Varian-Agilent PLGel mixed B column (25 cm in length, 4.6 mm ID) and HPLC-grade tetrahydrofuran (Wako Chemical, Osaka, Japan) as eluent at 30 °C on the basis of calibration with polystyrene standards (Tosoh, Tokyo, Japan). The intrinsic viscosity–molecular weight relationship was investigated at the Toray Research Centre (TRC, Shiga, Japan) using a Waters 1500 GPC apparatus with a Viscotec H502a viscometer (now, a member of Malvern group).

Dynamic force mode (DFM) images of atomic force microscopy (AFM) were captured using a SPA 400 SPM unit with a SII SPI 3800 probe station (Seiko Instruments, Inc., now, Hitachi High-Tech Science Corporation (Tokyo, Japan)). The sample was deposited onto an HOPG substrate (IBS-MikroMasch, Sofia, Burgaria; the Japanese vendor is Tomoe Engineering Co. (Tokyo, Japan)) by dropping the aggregate suspension in a mixture of methanol and toluene (= 1/1 (v/v)) and by drop-casting dilute chloroform solutions of **PF8** (0.5 x 10^{-5} M), **PSi-*S*** (1 x 10^{-5} M) and their mixtures in a mixture of methanol and chloroform (0.05–0.10 and 0.95–0.90 (v/v)). The deposited specimens were observed after the solvents were removed. Herein, we chose chloroform with a low bp (≈ 61°C) in place of toluene with a high bp (≈ 110 °C) to obtain good AFM images of these aggregates on HOPG.

Wide-angle X-ray diffraction (WAXD) data were collected by a Rigaku RINT-TTR III/NM instrument (Tokyo, Japan) using an X-ray wavelength of 1.5418 Å, CuKα radiation with Ni filter and $2\theta = 0.05°$ interval scan and scanning speed of 2 deg min^{-1}. The instrument was operated at 40 kV and 25 mA. Specimens onto an Si-crystal substrate were prepared by mixing **PF8** solid (M_n = 78,400), **PSi-*S*** solid (M_n = 75,800) and **PSi-*S*-PF8** (= 2:1 molar ratio) hetero-aggregate from chloroform-methanol (1/1 (v/v)) and from toluene-methanol (1/1 (v/v)). These specimens were dispersed in a high vacuum silicone grease (Dow-Corning-Toray).

The aggregate sizes were analysed by an Otsuka Electronics DLS-6000 dynamic light scattering (DLS) system (Hirakata-Osaka, Japan) with a detector angle of 90° and 30 accumulations using solution viscosity obtained with a Sekonic (Tokyo, Japan) viscometer VM-100 at 25 °C, along with the n_D value of methanol-toluene (1:1 (v/v)) at 589 nm at 25 °C using an Atago (Tokyo, Japan) thermo-controlled DR-M2 refractometer at 589 nm (Tokyo, Japan) at 20 °C.

For cryo-TEM (transmission electron microscopy) analysis, the aggregate suspension in methanol-toluene (1:1 (v/v)) was drop-cast onto a JEOL carbon-coated copper grid in 200 mesh (Akishima-Tokyo, Japan) and then directly exposed to liquid nitrogen. The high-resolution HR-TEM images were obtained on a Philips Tecnai G2 F20 S-TWINN electron microscope operated at an accelerating voltage of 200 kV.

Computer generated pentamer model of **PSi-*S*** with P-7_3 helix (dihedral angle ≈ 155°) and trimer model of **PF8** (dihedral angle ≈ 150°) were optimised with PM3-MM (Gaussian09 rev. D.01, Gaussian, Inc., Wallingford CT, 2013) running on an Apple PowerMac (2.67 GHz clock, 8-cores and 32 GB memory).

To measure the PL lifetime of **PF8**, we performed time-correlated single-photon counting (TCS-PC). The second harmonic (SHG = 420 nm) of a tunable Ti:sapphire laser (Coherent, Mira 900) with ≈ 150 fs pulse width and 76 MHz repetition rate was used as an excitation source. The PL emission was spectrally resolved using a collection of optics and a monochromator (Acton, SP-2150i). A TCSPC module (PicoHarp, PicoQuant) with an MCP-PMT (Hamamatsu, C4780) was used for ultrafast detection. The total instrument response function (IRF) for PL decay was less than 100 ps, which provided a temporal resolution of less than 10 ps. The deconvolution of the actual fluorescence decay and IRF was performed using fitting software (FlouFit, PicoQuant) to deduce the time constant associated with each exponential decay.

To photochemically decompose **PSi-*S*** (and **PSi-*R***) in the **PSi-PF8** hetero-aggregate suspension in a cuvette at room temperature, an ultra-high-pressure 500 W Hg lamp (Ushio (Tokyo, Japan), Optiplex BA-H501 and USH-500SC2) with a narrow band-pass filter of 313 nm (Asahi Spectra, Tokyo, Japan) was used. A photon flux at 313 nm was 14 μW cm^{-2} using an Si photodetector system (Ophir-Japan (Tokyo, Japan), Nova and PD300-UV). Details of the experimental set-up have been previously reported.[9a,9d]

3. Results and discussion

3.1. Chirality amplification from chiral PSi to achiral PF8

Fig. 2a shows the CD signals and broader UV-Vis spectra at approximately 399 nm that arise from α-phase **PF8**. The longest CD band and a sharper visible band at 435 nm were assigned to β-phase **PF8**.[4b,4f,6] An intense bisignate CD band at 305 and 322 nm was characteristic of exciton couplet arising from the helically assorted **PSi** aggregate.[4c,8,9b]

Our results indicate that the macromolecular helicity transfer is possible between helical non-charged **PSi** and non-helical non-charged **PF8** during the course of hetero-aggregation using a toluene-methanol cosolvent. For comparison, chloroform-methanol cosolvents with several ratios were possible to generate CD-/CPL active P**Si-*S*-PF8** hetero-aggregate though the absolute g_{CD} values of **PF8** slightly weakened. The helix scaffolds of **PSi-*S*** and **PSi-*R*** have a similar M_n of ≈ [illegible] exhibit nearly ideal mirror-image CD spectral characteristics with optically active **PF8**, in agreement with the characteristics previously reported for analogous chiral polymer systems.[2,4b,4d] The coexistence of highly emissive α- and β-phase **PF8** in the aggregates led to the detection of clear CPL signals and PL spectra arising from the β-phase,[4b,6] obeying a photoexcited energy migration scheme (ESI, Fig. S12). The CPL- and PL-bands are assigned to vibronic 0–0′ (438 nm), 0-1′ (464 nm) and 0-2′ (498 nm) bands with 1470–1490 cm^{-1} spacing due to aromatic ring stretching vibration of chiral β-phase,[4a,4b] as a result of spontaneous relaxation from the lowest S_1-state with $\nu = 0'$ to the S_0-state with $\nu = 0,1,2$ by the Kasha' rule.

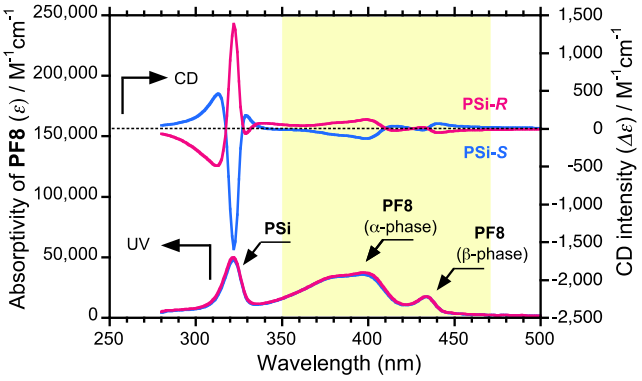

Fig. 2. CD and UV-Vis spectra of hetero-aggregates including **PSi-*S*** (**PSi-*R***) and **PF8** with a 2-to-1 ratio produced in a toluene-methanol cosolvent (1.5/1.5 (v/v)) with [**PF8**] = 2.5 × 10^{-5} M and [**PSi-*S***] = 5.0 × 10^{-5} M as their repeating units. The M_n values of **PSi-*S***, **PSi-*R*** and **PF8** are 75,800, 73,900 and 78,800, respectively.

3.2 Removal of PSi-*S* and PSi-*R* scaffolds

To spectroscopically elucidate the scaffolding capability of **PSi-*S*** and **PSi-*R*** toward **PF8**, the g_{CD} value of the hetero-aggregate suspension in a methanol-toluene cosolvent (1.5/1.5 (v/v)) was plotted as a function of the photoirradiation time at 313 nm, which is the optimal wavelength for excitation of the Si–Si* transition. To perform the polymer-selective photoscissoring experiment, we confirmed no oxidization of **PF8** aggregates by prolonged irradiation at 313 nm, as evident from no green PL band due to **PF8** keto form (Fig. 3b).[10] As evident in Fig. 3a, **PSi-*S*** decomposed rapidly within 60 s and completely disappeared within 300 s. The CD and CPL (Fig. 3b) amplitudes for **PF8** in **PSi-*S*-PF8**, which was photoirradiated for 600 s, nearly retained their initial g_{CD} (approximately ±0.005 at 401 nm) and g_{CPL} (approximately ±0.004 at 438 nm) magnitudes along with the chiroptical signs of **PF8** in the non-irradiated **PSi-PF8** (=2:1) aggregates. An approximately 10–20 % decrease in the g_{CD} magnitudes of **PF8** was observed after complete removal of **PSi-*R*** and **PSi-*S***. The **PSi**-selective photoscissoring reaction of the **PSi-PF8** hetero-aggregates was possible.

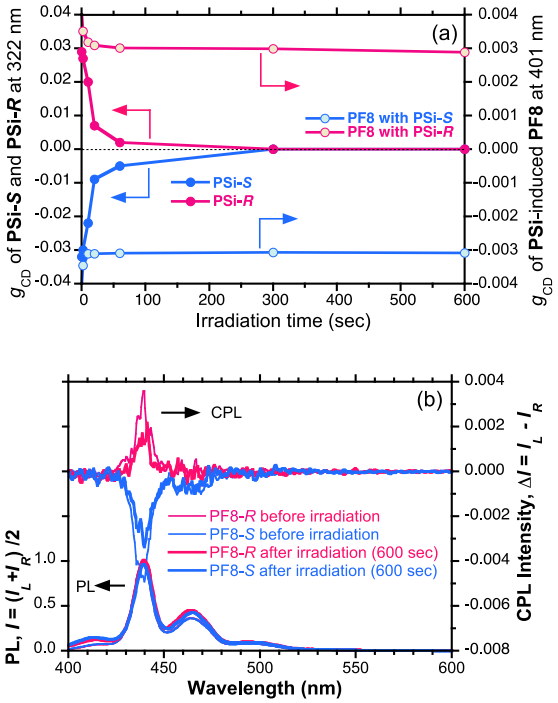

Fig. 3. Hetero-aggregates of **PF8** (2.5 × 10^{-5} M) and **PSi-*S*** (5.0 × 10^{-5} M) as a function of irradiation time at 313 nm (14 μW cm^{-2}). a) The g_{CD} values at 322 nm and 401 nm for **PSi-*S*** and **PF8** as a function of the irradiation time at 313 nm. b) CPL and PL spectra excited at 370 nm for the **PSi-*S*-PF8** and **PSi-*R*-PF8** aggregates before and after 313 nm irradiation for 600 s. The M_n values of **PSi-*S*, PSi-*R*** and **PF8** are 75,800, 73,900 and 78,800, respectively.

For further verification, a PL decay experiment of the **PSi-*S*-PF8** hetero-aggregate before and after photoscission was employed (Fig 4a). The PL decay curve due to β-phase **PF8** and its PL lifetime (τ [illegible] detected at [illegible] 480 [illegible]) were nearly unchanged before and after **PSi-*S*** selective photoscissoring at 313 nm for 600 s. The τ [illegible] value was slightly delayed from 2.37 to 2.46 ns. This result indicates that **PF8** maintained its original main chain structures even after prolonged UV irradiation, which resulted in photochemical removal of **PSi-*S*** as scaffolding. However, a helically assorted higher-order structure of **PF8** remained unchanged and was stable during the photochemical reaction.

The results of a DLS study strongly supported this conclusion (Fig. 4b). The hetero-aggregates caused division into two particles that were ≈ 2,000 nm (≈ 40 % by volume, relative to the original) and ≈ 300 nm in diameter in a fashion. This feature is similar to a cell division process even though the original material consisted of a single aggregate with a diameter of ≈ 2,730 nm. The 40 % reduction by volume was nearly equal to 49 % **PF8** by weight in the original **PSi-*S*-and-PF8** with a 2-to-1 ratio by repeat unit. The scissoring product of **PSi-*S*** was

assumed to be mostly concentrated in the 300 nm particles, whereas **PF8** mostly remained in the 2,000 nm particles. This result should provide a speculation that certain chiral species exist as sacrificial scaffolds in chemical evolution process of life and may catalyse the L-D preferences of biopolymers in μm-sized aggregate surrounded by aqueous medium,[1i] that is a model of coacervate coined by Oparlin and Haldane.

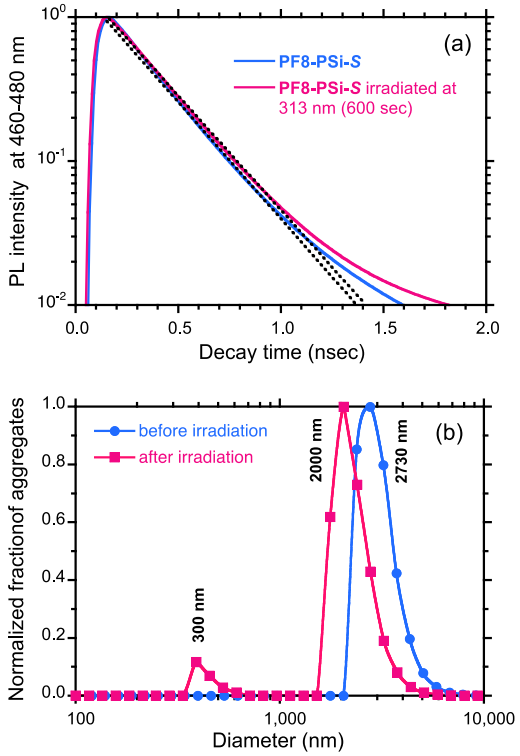

Fig. 4. (a) PL lifetime at 420 nm (excited by 150-fs pulse laser) of hetero-aggregates made of **PF8** (2.5×10^{-5} M) and **PSi-*S*** (5.0×10^{-5} M). (b) DLS data of the photobleached aggregates of **PF8** (2.5×10^{-5} M) and **PSi-*S*** (5.0×10^{-5} M) in a toluene-methanol cosolvent (1.5/1.5 (v/v)) before and after irradiation at 313 nm (14 μW cm^{-2}) for 600 s.

3.3 Optofluidic effect revealed as chiroptical amplification[4,9]

The cosolvent was optimised by optofluidically tuning n_D value and showed a great enhancement in the g_{CD} value of the hetero-aggregate at a specific n_D of ≈1.41 (Fig. 5), where the mixture of good and poor solvents (toluene and methanol) was 1 to 1 ratio (v/v). The detail of **PSi-*S*** CD-spectra was shown in ESI, Fig. S13. We are aware of the fact that the g_{CD}-n_D relationship shows a broad distribution for chiral **PSi** induced **PF8** particle. This indicates that **PSi-*S*** and **PF8** aggregate adopts a stable shape over a wide range of poor to good cosolvents.[11]

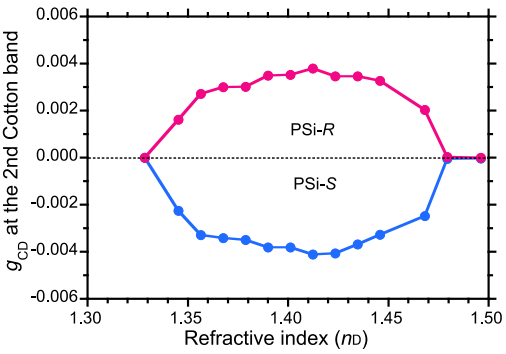

Fig. 5. The g_{CD} value of **PF8** at 401 nm in Toluene-MeOH cosolvents as a function of the refractive index (n_D) in the hetero-aggregate of the **PSi** and **PF8** molar ratio is = 5.0×10^{-5} M and 2.5×10^{-5} M. The M_n values of **PSi-*S*, PSi-*R*** and **PF8** are 75,800, 73,900 and 78,800, respectively.

However, improper ratio of good and poor solvents in the optofluidic medium may cause instability of the aggregate structures. Similar effect has been discussed in π-conjugated polymer, molecules and supramolecular polymer self-assembly systems experimentally and by computational modeling.[12]

3.4 Polymer molar ratio dependence

To gain additional insight into whether intermolecular interactions between **PSi-*S*** (**PSi-*R***) and **PF8** are stoichiometric, a Job's plot[13] was constructed for the **PSi**-**PF8** aggregates because such plots are useful for evaluating supramolecular complexes and applicable to polymer-polymer supramolecular complexes.[2h,2i,14,15] The g_{CD} value at the second Cotton band (401 nm) as a function of the molar ratio (as repeating unit) of **PF8**/[**PF8**+**PSi-*S***(**PSi-*R***)] is shown in Fig. 6a.

Surprisingly, the **PSi-*S***-and-**PF8** (and **PSi-*R***-and-**PF8**) hetero-aggregates preferentially adopt a 2-to-1 **PSi-PF8** ratio because the g_{CD} values reached a maximum at **PF8**/[**PF8**+**PSi-*S***] and **PF8**/[**PF8**+**PSi-*R***] of approximately 0.33. The hetero-aggregates do not obey the sergeant-and-soldier principle that is often observed in π-π stacked supramolecules and stiff helical copolymers.[14,16] Further analysis of the Job's plot indicated that the **PSi-PF8** hetero-aggregate is a supra-macromolecular complex with a 2-to-1 ratio (by repeating units) when the concentration of **PF8** is fixed to be 2.5×10^{-5} M (Fig. 6b). The 2-to-1 ratio is equivalent to 51:49 (by weight).

Recently, spontaneous generation of a similar supra-macromolecular triplex (so-called "stereocomplex") consisting of *isotactic* (*it*)- and *syndiotactic* (*st*)-poly(methyl methacrylate) (PMMA) with a 2-to-1 ratio was confirmed by HR-AFM and X-ray structural analyses.[14] The stereocomplex on HOPG, however, may exist as a mixture of *left*- and *right*-handed triple helices.

Notably, **PSi-*S*** and **PSi-*R***, in particular, adopt a rigid rod-like helical global conformation with high viscosity indices (α = 1.24 for **PSi-*S*** and α = 1.52 for **PSi-*R***) in toluene (ESI, Fig. S9–S11), which were confirmed by an extremely long persistent length that was as long as 85 nm (≈ 450 Si-repeating units, molecular mass of 96,000) in THF among a family of polysilanes.[5a] However, **PF8** adopts a semi-flexible CD-silent helical conformation with

substantial rotational freedom along the C–C bonds between the fluorene rings in the fluidic toluene solution. This result was confirmed by shorter persistent lengths of 10 nm at 25 °C and longer 34 nm at 50 °C.[6b] The combination of a highly rigid rod-like helix and semi-flexible CD-silent helical conformation may be critical for designing aggregation-induced scaffolding systems.

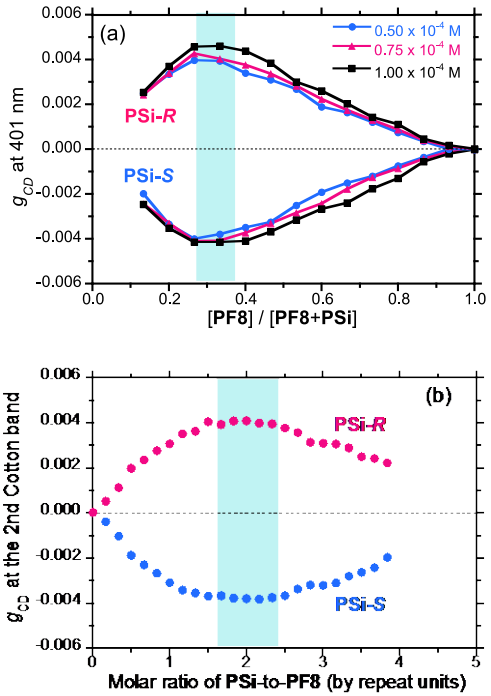

Fig. 6. a) Job's plot. The g_{CD} value of **PF8** as a function of the molar ratio of **PF8** in the hetero-aggregate. Three solution concentrations were tested: (0.50, 0.75, 1.00) × 10^{-4} M in toluene. b) The g_{CD} value of **PF8** at 401 nm as a function of the **PSi**-to-**PF8** molar ratio when $[\mathbf{PF8}]_0$ = 2.5 × 10^{-5} M.

3.5 Molecular weight dependence of helix scaffolding ability

Well-designed supramolecular architecture can promote a well-defined molecular interaction when the two bodies are adhering together. This interaction should be closely related to spontaneously an assembling process.[17] To clarify whether M_n values of **PF8** and **PSi** values affect the **PSi-and-PF8** scaffolding capability, we examined the g_{CD} value of **PSi-and-PF8** with 2-to-1 hetero-aggregates as functions of M_n values of **PF8** and **PSi-*S*** in detail. Four **PF8** samples with *PDI* ≈ 1.7–2.0 and six **PSi-*S*** samples with *PDI* ≈ 1.3–1.5 were isolated by an ordinary fractionation method with IPA, ethanol and methanol as precipitating solvents (Tables 1 and 2). For comparison, one **PSi-*R*** sample with *PDI* ≈ 1.3 was used.

From irradiation time dependence at 313 nm to **PSi-*S*-PF8** aggregates, the g_{CD} value of the hetero-aggregates greatly depended on M_n value of **PSi-*S*** when **PF8** with M_n = 82,800 was fixed (Fig. 7a). It is evident that, among six **PSi-*S*** samples, the g_{CD} value afforded the maximum one when **PSi-*S*** is M_n = 40,500 before and after the 313-nm irradiation. Thus, the g_{CD} value did not monotonically increase as M_n value of **PSi-*S*** increases (Fig. 7b). The scaffolding capability is crucial in providing an ideal intermolecular interaction between **PF8** and **PSi-*S***. On the other hand, the g_{CD} value of **PSi-*S*-PF8** aggregate monotonically increases and tends to reach level-off g_{CD} values when the M_n value of **PSi-*S*** ranges from 9,800 and 80,400 (Fig. 7c). The g_{CD} value of **PSi-*S*-PF8** aggregate weakly depends on M_n value of **PF8**.

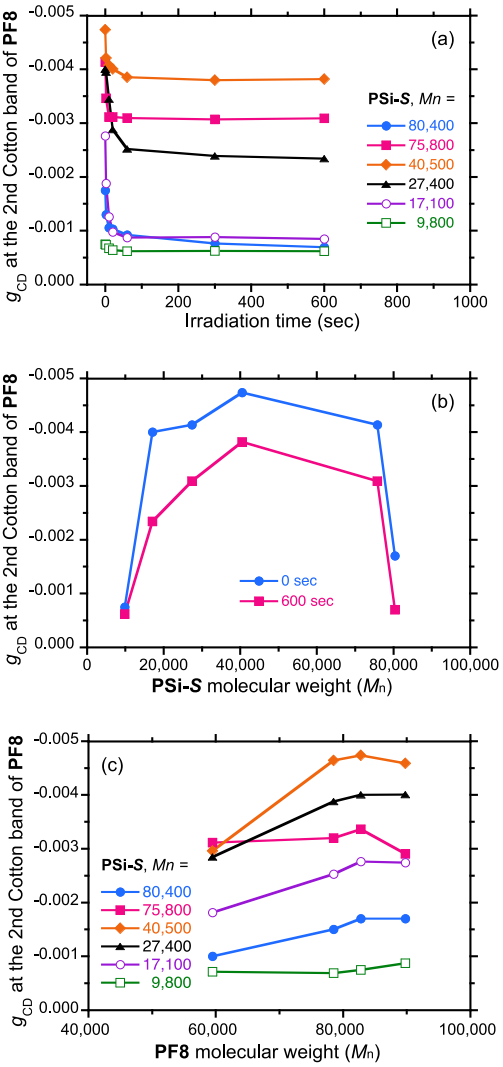

Fig. 7. a) The g_{CD} value of **PF8** at 401 nm using **PSi-*S*** with different molecular weight and **PF8** (M_n = 82,800) hetero-aggregates with a 2-to-1 ratio produced in a toluene-methanol cosolvent (1.5/1.5 (v/v)) with $[\mathbf{PF8}]$ = 2.5 × 10^{-5} M and $[\mathbf{PSi\text{-}S}]$ = 5.0 × 10^{-5} M as the repeating units and as a function of the irradiation time at 313 nm (14 μW cm^{-2}). b) The g_{CD} value at 401 nm of **PSi-*S*-PF8** aggregate as a function of **PSi-*S*** before and after irradiation time at 313 nm (14 μW cm^{-2}) for 600 s. c) The g_{CD} value at 401 nm of **PSi-*S*-PF8** hetero-aggregates (2-to-1 ratio produced in a toluene-methanol cosolvent (1.5/1.5 (v/v)) with $[\mathbf{PF8}]$ = 2.5 × 10^{-5} M and $[\mathbf{PSi\text{-}S}]$ = 5.0 × 10^{-5} M as their repeating units) as a function of both M_n values with **PF8** and **PSi-*S***.

A pair of two different linear polymers with the oppositely charged pairs may promote a better electrostatic interaction as their main-chain lengths increase, due to sufficient intermolecular locking.[18] However, in the case of pair of non-charged polymers, the semi-flexible **PF8** may gradually loose the wrapping capability toward rod-like **PSi-*S*** above the critical M_n ≈ 80,000. On the other hand, rod-like **PSi-*S*** efficiently acts as an efficient scaffold toward semi-flexible **PF8** regardless of M_n of **PSi-*S*** ranging from 9,800 and 80,400. The scaffolding ability of **PSi-*S*** is kept during photochemical scissoring reaction of Si–Si bonds.

To further consider which factor among molecular weight, main-chain length and DP_n is critical factor to afford the best scaffolding ability and to discuss the reason why the best **PSi-*S*-PF8** aggregate with the greatest g_{CD} value prefers the 1-to-2 ratio as repeating units (Fig. 6), we evaluated main chain lengths and DP_n values of **PF8**, **PSi-*S*** and **PSi-*R*** from the corresponding M_n values (Tables 1 and 2).

Table 1. Molecular weights, polydispersity, main chain length and number-average degree of polymerization of **PF8**.

Fraction	M_n	M_w/M_n	Length of **PF8** (in nm)	DP_n
1	89,800	2.0	194	230
2	82,800	1.8	179	**212**
3	78,400	2.1	169	201
4	59,500	1.7	129	152

Table 2. Molecular weights, polydispersity, main chain length and number-average degree of polymerization of **PSi-*S*** and **PSi-*R***.

Chiral centre	M_n	M_w/M_n	Length of **PSi** (in nm)	DP_n
S	80,400	1.4	57	436
S	75,800	1.5	54	411
R	73,900	1.3	53	401
S	40,500	1.5	29	**220**
S	27,400	1.4	20	149
S	17,100	1.3	12	93
S	9,800	1.5	7	53

The stoichiometry as repeating units of **PF8** and **PSi** is a critical factor for the hetero-aggregate, in which **PF8** with $DP_n \approx 212$ matches **PSi-*S*** with $DP_n \approx 220$ in the range of $DP_n = 50$ and 436. CD- and UV-vis spectra of the **PSi-*S*** selective photobleached **PSi-*S*-PF8** aggregate were provided in ESI, Figs. S16a and S16b. Actually, the nearly identical DP_n values of **PSi-*S*** and **PF8** afforded the highest g_{CD} amplitude that attains ≈ –0.005 at 438 nm of **PF8**.

Previously, Harada and Kataoka[18] demonstrated that a precisely controlled main chain length of charged polymers helps to produce a highly ordered supramolecular assembly, resulting in a core-shell structure. In addition to main chain length, they found that the degree of polymerization (*DP*) plays a key role in constructing the self-assembling structure with the oppositely charged polymers, that is polyion complex. In this case, all the polymers had an extreme narrow *PDI* < 1.1. Their knowledge and understanding might be applicable to supramolecular complexation between two non-charged **PF8** and **PSi**. The best matched DP_n values between **PF8** and **PSi** is responsible for the supramolecular hetero-aggregation. This idea could be applicable to complexations between two polar polymers and between nonpolar polymers, as well as between the oppositely charged polymers

An open question is why the 2-to-1 ratio is the best for the **PSi-*S*-and-PF8** aggregates. Noted that each **PF8** repeating unit has two *n*-octyl side chains at 9,9-position (eight carbons × 2 = sixteen carbons), whilst each **PSi-*S*** repeating unit has single *n*-hexyl side chain (six carbon × 1). A plausible answer is that two *n*-octyl side chains of **PF8** repeating unit interact with two units of **PSi-*S*** carrying one *n*-hexyl side chain, enabling an efficient interaction of these *n*-alkyl side chains. To build a supramolecular structure, more longer alkyl side chains of polyfluorene derivatives will be needed to efficiently wrap around the rigid rod-like **PSi-*S*** helical main chains.

3.6. WAXD study of PSi-*S*, PF8 and PSi-S-and-PF8 with 2:1 ratio

We compared the WAXD profiles between **PSi-*S*-PF8** (1:2) hetero-aggregate and the corresponding **PF8** and **PSi-*S*** homo-aggregates (Fig. S14, ESI). The WAXD profile of **PSi-*S*-PF8** hetero-aggregate had three characteristic *d*-spacing at 4.4 Å, 7.5 Å and 12.4 Å. The 12.4 Å spacing is ascribed to interchain distance of **PSi-*S***. However, the origin of 4.4 Å and 7.5 Å spacing is obscure because these are commonly seen among three aggregates. However, the WAXD profile of **PSi-*S*-PF8** hetero-aggregate subtly depended on sample preparation condition whether the aggregate was casted from toluene-methanol (1/1 (v/v)) or chloroform-methanol (1/1 (v/v)) (Fig. S15, ESI). The 12.4 Å spacing became 12.2 Å when chloroform was employed. The 7.5 Å spacing shortened by ≈ 0.8 Å and became ≈ 6.7 Å when chloroform was employed. The 4.4 Å spacing was unchanged.

The reductions of 0.2 Å and 0.8 Å in the hetero-aggregates implied certain interactions between **PF8** and **PSi-*S***, depending on solvent condition. However, we did not obtain more useful information about these aggregates due to limited availability of clear X-ray scattering peaks. Helical pitch of polymers is susceptible to external physical and chemical biases. Recently, Knaapila *et al* reported that high hydrostatic pressure largely affects helical pitch of poly[9,9-bis(2-ethylhexyl)fluorene].[10d]

3.7. TEM and AFM studies of PSi-*S*, PF8 and PSi-S-and-PF8

We attempted to view the detailed structures of **PF8** and **PSi-*S*** homo-aggregates and **PSi-*S*-and-PF8** hetero-aggregates using cryogenic transmission electron microscopy (cryo-TEM) (ESI, Fig. S17). Because of rapid scissoring reaction of the Si–Si backbone over the TEM observation time, clear visualisation was impossible even at liquid-nitrogen temperature. Then, we employed DFM-AFM study because of no sample damage.

The first approach was applied to view DFM-AFM images of **PSi-*S*** and **PF8** homo-aggregates and **PSi-*S*-and-PF8** hetero-aggregates. These specimens were directly deposited onto HOPG by drop-casting the aggregates suspension in 10^{-4} M toluene-methanol (1/1 (v/v)). However, we did not obtain clearer assorted images (ESI, Fig. S18).

The second approach was to use chloroform as a good solvent including a small volume fraction of methanol. We obtained better resolution AFM images of **PSi-*S*** and **PF8** homo-aggregates on HOPG by a drop-cast of their very dilute

chloroform solutions (10^{-5} M) (ESI, Fig. S19–S22). Similarly, **PSi-*S*-and-PF8** hetero-aggregate (as nominal ratio of 2-to-1) was casting from their dilute solution (≈ 10^{-5} M) of 5 % methanol and 95 % chloroform (ESI, Fig. S23). The choice of volatile chloroform was the key to yield better AFM images rather than less-volatile toluene.

From several height profiles of Fig. S19 in ESI, diameters of **PSi-*S*** casting from pure chloroform solution ranged from ≈ 0.5 and ≈ 1.1 nm on HOPG. These heights are nearly consistent with diameters of individual **PSi-*S*** chains that laterally aligned on HOPG surface. Two representative molecular diameters of 7_3-helical **PSi-*S*** were given in Fig. S19 in ESI. One motif is stretch out structure of *n*-hexyl side groups with *all-trans* geometry and the other one is its shrunk shape with *gauche* form. The height value of 1.1 nm is nearly identical to *d*-spacing (12.2 and 12.4 Å) of **PSi-*S*** solid (ESI, Figs. S15 and S16). A combined data of the WAXD and AFM images suggested that *n*-hexyl groups adopt the shrunk geometry on HOPG. An averaged end-to-end distance of **PSi-*S*** arrays on HOPG was ≈ 31 nm. This value corresponds to ≈ 170 Si-repeating units, but is one-third of DP_n (= 458) evaluated by GPC analysis (Table 2). However, we could not clearly view a helical molecular image of **PSi-*S*** on HOPG. This is probably due to an AFM tip broadening effect since the current AFM tip size (2–5 nm) was comparable with 7_3-helical pitch (1.3–1.5 nm) of **PSi-*S***.

In the presence of methanol in chloroform, the cross-section values of **PSi-*S*** drastically increased. The cross-section obtained from 5 % methanol and 95 % chloroform is in the range of ≈ 3.5 nm and ≈ 5.0 nm, that are equivalent to 5–7 molecular thickness of **PSi-*S*** (ESI, Fig. S20). The cross-section after removal of 10 % methanol and 90 % chloroform was in the range of 8 nm and 11 nm, yielding 11–15 molecular thickness of **PSi-*S*** (ESI, Fig. S21). These AFM images clearly indicated that **PSi-*S*** spontaneously forms aggregates on HOPG with help of methanol as an aggregation inducing solvent. Possibly, C-H(**PSi-*S***)/π(HOPG) and London dispersion interactions are responsible for the aggregation. The aggregate size and height of **PSi-*S*** largely depended on the initial volume fraction of methanol. Plausible helically assorted **PSi-*S*** on HOPG was illustrated in Figs. S20 and S21 in ESI.

On the other hand, height profiles of **PF8** obtained with from 5 % methanol and 95 % chloroform ranged from ≈ 0.5 nm and ≈ 2 nm (ESI, Fig. S22). When one can assume stretch out structure of two *n*-octyl groups with *all-trans* geometry, an estimated end-to-end distance of two side groups is ≈ 2.0 nm and thickness of **PF8** rings is ≈ 0.5–0.7 nm. Because of semi-flexible nature, **PF8** chains can turn into ill-defined, highly entangling organization on HOPG, including face-one, edge-on and loop-train-tail structures as outlined in ESI, Fig. S22, bottom right.

Finally, height profiles of **PSi-*S*** and **PF8** aggregates obtained with 5 % methanol and 95 % chloroform tells us that the aggregates had an almost uniform cross-section height ranging from 5.5 and 6.1 nm (ESI, Fig. S23). These images suggested that **PSi** chains and **PF8** chains spontaneously co-aggregated with 2-to-1 ratio on HOPG during co-evaporation of chloroform and methanol. The AFM images are not segregated structures of **PSi** and **PF8**. The height of ≈ 6 nm corresponds to two **PSi** chains interacted with two *n*-octyl groups of two **PF8** chains, as illustrated in ESI, Fig. S24, top.

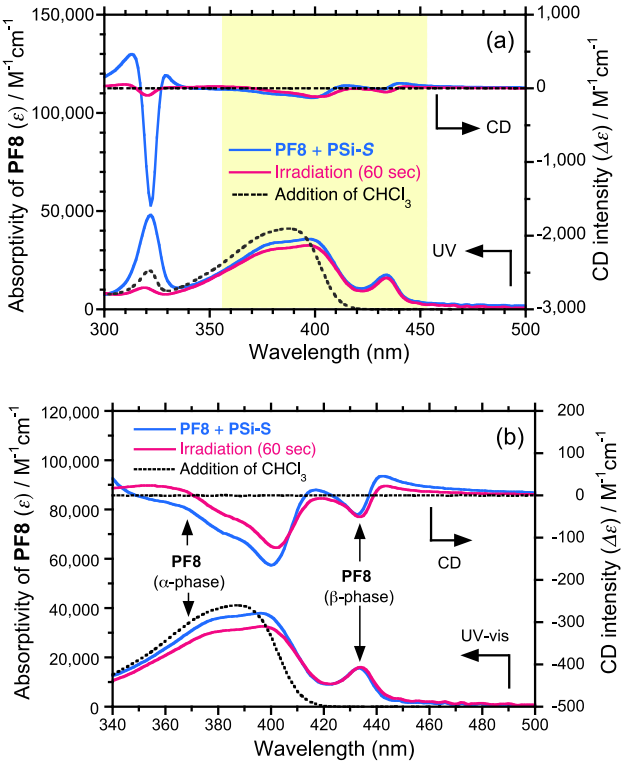

Fig. 8. (a) CD and UV-Vis spectra and (b) magnified spectra of the photobleached aggregates of **PF8** (2.5×10^{-5} M) and **PSi-*S*** (5.0×10^{-5} M) dissolved in a homogeneous chloroform solution as well as the original and photobleached aggregate suspension for comparison in a toluene-methanol cosolvent (1.5/1.5 (v/v)) before and after irradiation at 313 nm (14 μW cm^{-2}) for 60 s.

Additionally, we viewed two heights of ≈ 1.5 nm and ≈ 3 nm, depending on position of AFM tip. These heights may be ascribed to two **PSi** chains and two **PSi** chains with one-side of one **PF8** chain, respectively (ESI, Fig. S24, bottom). Although we cannot obtain a clear helical AFM image of the hetero-aggregates, several alkyl side chains between **PSi** and **PF8** are assumed to be interdigitated and coagulated. In this case, we postulated that two helical **PSi-*S*** chains form a double strand that is loosely wrapping by one **PF8** chain. The double strand **PSi-*S*** is responsible for the intense exciton couplet CD signals at 310–320 nm[4c,9b] (Fig. 2 and ESI, Fig. S25). From the AFM images, the twisted, but more planarised **PF8** aggregate suspension in the cosolvents might be responsible for CD-/CPL-active *β*-phase at 434 nm[4a,4b] (Fig. 2 and ESI, Fig. S26).

3.8 Possible interactions between non-charged PSi and PF8

Two unanswered questions still remained: (i) Does the CPL- and CD-activities of the **PSi**-selective photobleached **PF8** aggregates arise from intermolecular covalent bonds with a photodecomposed moiety of **PSi** or from only non-covalent interactions? And (ii) what type of intermolecular interactions between **PF8** and **PSi** is responsible for the scaffolding capability?

To address the first question, we measured the CD and UV-Vis spectra of a homogeneous chloroform solution containing photobleached aggregates of **PSi-*S*-PF8** (=2:1). Figs. 8a-8b show the CD and UV-Vis spectra of the photobleached aggregates (313 nm, 60 s) of **PSi-*S*-PF8** (=2:1) by adding chloroform; for comparison, the spectra of the corresponding original and photobleached **PSi-*S*-PF8** aggregates in toluene-methanol cosolvent (1.5/1.5 (v/v)) before and after 313 nm irradiation for 60 s are also shown. The CD and UV-Vis bands of the α-phase (≈ 350 and ≈400 nm) and β-phase (≈ 433 nm) of **PF8** completely disappeared in chloroform. Intermolecular crosslinking reactions did not occur in the aggregate during the photoscissoring process. The predicted silyl radical species[5b] did not contribute to the maintenance of the CD and CPL activities in the **PSi-*S*-PF8** aggregate.

Regarding the second question, we assume that H/H interactions (coined dihydrogen bonds) exist in the dimer of the saturated hydrocarbons as an extension of CH/π and London dispersion interactions.[20] This proposal was based on rigorous calculations at the second-order Møller-Plesset (MP2) level with the 6-311++G(3df,3pd) basis set. In methane dimers, the stabilisation energy arises from the weakly charged C^{-}-H^{+}/H^{-}-C^{+} pair in the valance bond; in particular, the positioning of the neighbourhoods is critical. Staggered and eclipsed triple H/H contacts of the CH_3/H_3C pair had a dissociation energy of 1.6−1.8 kJ mol^{-1}, and the staggered and eclipsed double H/H contacts of the CH_2/H_2C pair had a dissociation energy of 1.0−1.4 kJ mol^{-1}.[20]

However, in *n*-alkane dimers, a staggered supramolecule with 3:3 and 1:1 contacts asymptotically stabilises as the methylene number increases. The dissociation energy plateaued at six methylenes, reaching 1.56 and 2.40 kJ mol^{-1}, respectively.[20]

Recently, Hariharan *et al*. reported experimentally and computationally that, in crystals of pyrenes substituted with acetyl and anthracene groups, the attractive H/H interactions between sp^2 C–H of pyrene and sp^3 C–H of methyl (from of acetyl) and between sp^2 C–H of pyrene and sp^2 C–H of anthracene with help of CH/π interaction facilitate to generate specific organisations such as herringbone, brickwork and columnar structures.[21]

These fascinating outcomes led us to propose that the minimal carbon number in the *n*-alkane dimer is six. Therefore, multiple attractive C-H/H-C interactions between the two *n*-octyl groups (**PF8**) and the *n*-hexyl group (**PSi-*S*** and **-*R***) are sufficiently strong for scaffolding capability, irrespective of the absence of electrostatic, hydrogen-bonding, dipole-dipole, CH/π, CH/N, CH/O and π/π interactions. Our preliminary study indicated the best *n*-alkyl side-chain length pair between **PF8** and **PSi** exists, enabling a more enhanced scaffolding capability with high g_{CD} values.

Various supramolecular polymer complexes using single- and two-components of molecular and oligomeric building blocks are promising to design (chir)optical, semiconducting, and biological functions as well as well-defined, higher-order fibrous and gel structures.[22] Rather directional, intense hydrogen, π-π stacking and electron donor-acceptor interactions are driving forces for these well-defined, higher-order fibrous structures.

As demonstrated in this work, even non-directional weak interactions can contribute to supra-macromolecular complexation comprising non-charged, non-polar π- and σ-conjugated polymers though the resultant hetero-aggregate had a difficulty to characterize a detailed structure due to ill-defined structures. Nevertheless, our approach is beneficial to more freely design solution processible supramolecular complexation of two non-charged macromolecules with sophisticated (chir)optical, electronic and other functions.

Actually, in a series of preliminary experiments, we confirmed that the aggregation-induced scaffolding with **PSi-*S*** and **PSi-*R*** is valid for commonly generate CD- and CPL-active π-conjugated polymers including poly[(9,9-di-*n*-octylfluoren-2,7-diyl)-*alt*-bithiophene] (**PF8T2**),[4a] poly[(9,9-di-*n*-octylfluoren-2, 7-diyl)-*alt*-ylene-ethynylene] (**PPE**),[9c] poly(9,9-*n*-dioctyl-fluorene-2,7-vinylene) (**PFV**),[9c] and so on. Even **PPE** was converted into the corresponding CD-/CPL-active aggregates with help of **PSi-*S*** though limonene was inefficient as the chiral liquid scaffold.[9c] The works are currently in progress.

3.9 Hetero-aggregation scenario of PSi and PF8

Based on the above experimental results, herein, we proposed a possible scenario of emerging CD-/CPL-active **PF8** aggregate when CD-/CPL-silent **PF8** was employed with **PSi-*S*** as a helix scaffold (Figure 9), as follows.

Stage I. In good solvents (toluene and chloroform), semi-flexible **PF8** has a rich conformational freedom along C–C single bonds between fluorene rings, whereas **PSi-*S*** adopts a rigid 7_3-helical structure due to restricted rotation of Si–Si single bonds. Long *n*-hexyl and *n*-octyl side chains are fully interacted with solvents and should adopt a fairly stretch out geometry.

Stage II. By changing from pure good solvent to poorer cosolvent by employing a slow addition of methanol, **PSi-*S*** preferentially self-assembles to a higher-order helical structure, while **PF8** exists as individual polymer chain even in the poorer cosolvent. The key factor is that **PSi-*S*** possesses an intense self-aggregation ability relative to **PF8**, arising from great differences in main chain rigidity and solubility in the solvent. In this case, *n*-hexyl groups should adopt a shrunk geometry.

Stage III. From the poorer to definitively poor cosolvents by further addition of methanol, the higher-order **PSi-*S*** helical motif causes a complexation with **PF8** due to its limited solubility in the poor solvent. Multiple C-H/H-C interactions between *n*-hexyl groups of **PSi-*S*** and *n*-octyl groups of **PF8** are responsible for the attractive macromolecular complexation. In this case, matching in side chain lengths of **PSi-*S*** and **PF8** is another critical factor. Then, **PSi-*S*** helicity is efficiently transferred to **PF8** due to a great loss of conformational freedom, yielding CD-/CPL-active, but metastable β-phase **PF8** hetero-aggregate kept by rigid **PSi-*S*** helicity. The metastablity was confirmed by complete loss of CD signal of **PF8** when chloroform was added to the hetero-aggregate.

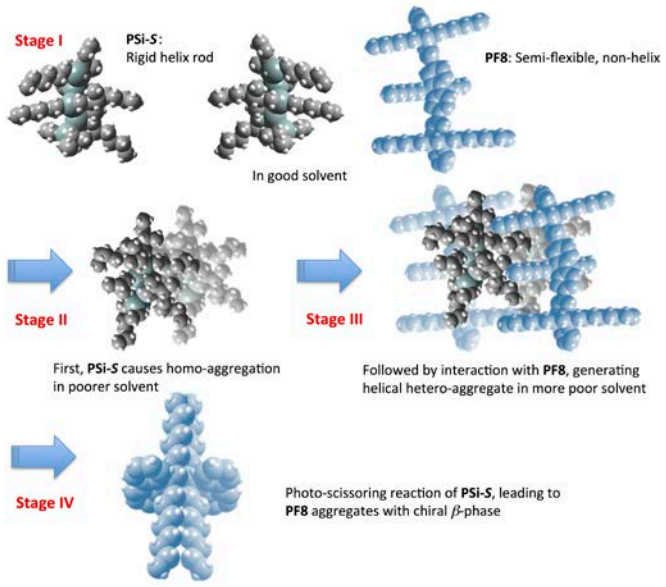

Fig. 9. Scenario of **PSi-*S*** helicity transfer to generate helical β-phase **PF8** during hetero-aggregation of **PSi-*S*** and **PF8**, followed by removal of **PSi-*S*** scaffold by **PSi-*S*** selective photoscissoring reaction in poor solvents.

Stage IV. The hetero-aggregate consisting of **PSi-*S*** and **PF8** turns to CD-/CPL-**PF8** aggregate after a complete removal of **PSi-*S*** as a helix scaffold by photoscissoring reaction at Siσ-Siσ* transition. In this case, **PF8** chains turn into thermodynamically stable chiral β-phase. The chiral β-phase **PF8** structures are stabilised through multiple C-H/H-C interactions between *n*-octyl groups.

4. Conclusion

In conclusion, we have reported the first photochemically controlled scaffolding of hetero-aggregates consisting of **PSi** and **PF8** via a **PSi**-selective photoscissoring reaction. This protocol allowed for the successful production of a CPL- and CD-active **PF8** aggregate by complete removal of **PSi**. Surprisingly, the hetero-aggregates may be a supra-macromolecule consisting of two **PSi** chains and one **PF8** chain. We assumed that sufficiently strong attractive C-H/H-C interactions existing between two *n*-octyl groups of **PF8** and one *n*-hexyl group of **PSi** are responsible for scaffolding capability, regardless of the absence of electrostatic, hydrogen-bonding, dipole-dipole, CH/π, CH/N, CH/O and π/π interactions.

5. Acknowledgements

MF acknowledges financial support from JSPS KAKENHI (16H04155). NAAR acknowledges financial support from the NAIST Presidential Special Fund. NAAR wishes to thank Profs. Hiroshi Daimon, Hiroko Yamada and Jun-ichi Kikuchi for fruitful discussion and valuable comments. Also, we thank Dr. Nozomu Suzuki, Sibo Guo and Keisuke Yoshida for stimulating discussion. Kazuhiro Miyake (AFM), Yoshiko Nishikawa (DLS), Sakiko Fujita (cryo-TEM and HR-TEM) and Yasuo Okajima (PL lifetime) helped us technically. The authors gratefully acknowledge three anonymous reviewers for valuable suggestions, allowing us to largely improve the original manuscript with several additional experiments.

6. Notes and references

1 For reviews. a) M. Liu, L. Zhang and T. Wang, *Chem. Rev*. 2015, **115**, 7304; b) W. A. Bonner, *Orig. Life Evol. Biosph.* 1992, **21**, 407; c) Y. Inoue, *Chem. Rev*., 1992, **92**, 741; d) J. K. Barton, 1986, *Science.*, **233**, 727; e) S. F. Mason, *Nature*, 1984, **311**, 19; f) A. Córdova, M. Engqvist, I. Ibrahem, J. Casa, H. Sundén, *Chem. Commun*., 2005, 2047; g) I. Sato, H. Urabe, S. Ishiguro, T. Shibata, K. Soai, *Angew. Chem. Int. Ed*., 2003, **42**, 315; h) T. Kawasaki, M. Sato, S. Ishiguro, T. Saito, Y. Morishita, I. Sato, H. Nishino, Y. Inoue, and K. Soai, *J. Am. Chem. Soc*., 2005, **127**, 3274; i) M. Fujiki, K. Yoshida, N. Suzuki, N. A. A. Rahim and J. A. Jalil, *J. Photochem. Photobiol. A. Chem*., 2016 DOI (http://dx.doi.org/10.1016/ j.jphotochem.2016.01.027).

2 a) J. Glowacki and S. Mizuno, *Biopolymers*, 2008, **89**, 338; b) S. Le Gac, E. Schwartz, M. Koeph, J. J. L. M. Cornelissen, A. E. Rowan and R. J. M. Nolte, *Chem. Eur. J*., 2010, **16**, 6176; c) J. D. Le, Y. Pinto, N. C. Seeman, K. Musier-Forsyth, T. A. Taton and R. A. Kiehl, *Nano Lett.*, 2004, **4**, 2343; d) Y.-M. Guo, H. Oike and T. Aida, *J. Am. Chem. Soc.*, 2004, **126**, 716; e) G. Fukuhara, K. Iida, Y. Kawanami, H. Tanaka, T. Mori and Y. Inoue, *J. Am. Chem. Soc.*, 2015, **137**, 15007; f) D. J. Hill, M. J. Mio, R. B. Prince, T. S. Hughes and J. S. Moore, *Chem. Rev.*, 2001, **101**, 3893; g) E. Schwartz, L. G. Stephane, J. J. L. M. Cornelissen, R. J. M. Nolte and A. E. Rowan, *Chem. Soc. Rev*., 2010, **39**, 1576; h) T. Shiraki, Y. Tsuchiya, T. Noguchi, S.-i. Tamaru, N. Suzuki, M. Taguchi, M. Fujiki and S. Shinkai, *Chem. Asian J.*, 2014, **9**, 218; i) T. Shiraki, A. Dawn, Y. Tsuchiya and S. Shinkai, *J. Am. Chem. Soc.*, 2010, **132**, 13928; j) S. Haraguchi, M. Numata, C. Li, Y. Nakano, M. Fujiki and S. Shinkai, *Chem. Lett.*, 2009, **38**, 254; k) M. Ikeda, T. Hasegawa, M. Numata, K. Sugikawa, K. Sakurai, M. Fujiki and S. Shinkai, *J. Am. Chem. Soc.*, 2007, **129**, 3979; l) E. Yashima, K. Maeda and Y. Okamoto, *Nature*, 1999, **399**, 449.

3 a) Y. Ono, K. Nakashima, M. Sano,Y. Kanekiyo, K. Inoue, J. Hojo and S. Shinkai, *Chem. Commun*., 1998, 1477; b) Y. Yang, M. Suzuki, S. Owa, H. Shirai and K. Hanabusa, *J. Mater. Chem*., 2006, **16**, 1644; c) D. Liu, B. Li, Y. Guo, Y. Li, and Y. Yang, *Chirality*, 2015, **27**, 809; d) D. Yang, Y. Zhao, K. Lv, X. Wang, W. Zhang, L. Zhang and M. Liu, *Soft Matter*, 2016, **12**, 1170; e) R. Tamoto, N. Daugey, T. Buffeteau, B. Kauffmann, M. Takafuji, H. Ihara and R. Oda, *Chem. Commun.*, 2015, **51**, 3518.

4 a) K. Kawagoe, M. Fujiki and Y. Nakano, *New J. Chem*. 2010, **34**, 637; b) Y. Nakano, Y. Liu and M. Fujiki, *Polym. Chem.*, 2010, **1**, 460; c) Y. Nakano, F. Ichiyanagi, M. Naito, Y.-G. Yang and M. Fujiki, *Chem. Commun*., 2012, **48**, 6636; d) L. Wang, N. Suzuki, J. Liu, T. Matsuda, N. A. A. Rahim, W. Zhang, M. Fujiki, Z. Zhang, N. Zhou and X. Zhu, *Polym. Chem*. 2014, **5**, 5920; e) H. Nakashima, J. R. Koe, K.Torimitsu and M. Fujiki, *J. Am. Chem. Soc*., 2001, **123**, 4847; f) Y. Zhao, N. A. A. Rahim, Y. Xia, M. Fujiki, B. Song, Z. Zhang, W. Zhang and X. Zhu, *Macromolecules*, 2016, **49**, 3214; g) For a review, M. Fujiki, *Symmetry*, 2014, **6**, 677.

5 a) M. Fujiki, J. R. Koe, K. Terao, T. Sato, A. Teramoto and J. Watanabe, *Polym. J.*, 2003, **35**, 297; b) R. D. Miller and J. Michl, *Chem. Rev*., 1989, **89**, 1359; c) A. Saxena, K. Okoshi, M. Fujiki, M, Naito, G. Q. Guo, T. Hagihara and M. Ishikawa, *Macromolecules*, 2004, **37**, 367.

6 a) U. Scherf and E. J. W. List, *Adv. Mater.*, 2002, **14**, 477; b) J.-H. Chen, C.-S. Chang, Y.-X. Chang, C.-Y. Chen, H.-L. Chen and S.-A. Chen, *Macromolecules*, 2009, **42**, 1306; c) M. Oda, H. G.

Nothofer, U. Scherf, V. Sunjic, D. Richter, W. Regenstein and D. Neher, *Macromolecules*, 2002, **35**, 6792; d) M. Knaapila, V. M. Garamus, F. B. Dias, L. Almasy, F. Galbrecht, A. Charas, J. Morgado, H. D. Burrows, U. Scherf and A. P. Monkman, *Macromolecules*, 2006, **39**, 6505; e) M. Knaapila and A. P. Monkman, *Adv. Mater*., 2013, **25**, 1090.

7 a) For a review, Y. Hong, J. W. Y. Lam and B. Z. Tang, *Chem. Soc. Rev*., 2011, **40**, 5361; b) A. Ajayaghosh, R. Varghese, S. Mahesh, V. K. Praveen, *Angew. Chem. Int. Ed., 2006,* **45**, 7729; c) J. Luo, Z. Xie, J. W. Y. Lam, L. Cheng, H. Chen, C. Qiu, H. S. Kwok, X. Zhan, Y. Liu, D. Zhu and B. Z. Tang, *Chem. Commun.*, 2001, 1740.

8 E. L. Eliel, S. H. Wilen and L. N. Mander, *Stereochemistry of Organic Compounds*, *Chapter 13. Chiroptical Properties*, Wiley-Interscience, New York (NY), 1994.

9 a) M. Fujiki, K. Yoshida, N. Suzuki, J. Zhang, W. Zhang and X. Zhu, *RSC Adv*., 2013, **3**, 5213; b) Y. Nakano and M. Fujiki, *Macromolecules*, 2011, **48**, 7511; c) M. Fujiki, A. J. Jalilah, N. Suzuki, M. Taguchi, W. Zhang, M. M. Abdellatif and K. Nomura, *RSC Adv*., 2012, **2**, 6663; d) M. Fujiki, Y. Donguri, Y. Zhao, A. Nakao, N. Suzuki, K. Yoshida, W. Zhang, *Polym. Chem*., 2015, **6**, 1627 and references cited therein.

10 a) E. J. W. List, R. Guentner, P. S. de Freitas and U. Scherf, *Adv. Mater*., 2002, **14**, 374; b) T. Shiraki, S. Shindome, F. Toshimitsu, T. Fujigaya and N. Nakashima, *Polym. Chem.*, 2015, **6**, 5103; c) L. Zaikowski, P. Kaur, C. Gefind, E. Selvaggio, S. Asaoka, Q. Wu, H. C. Chen, N. Takeda, A. R. Cook, A. Yang, J. Rosanelli and J. R Miller, *J. Am. Chem. Soc.*, 2012, **134**, 10852; d) M. Knaapila, Z. Konopkova, M. Torkkeli, D. Haase, H. -P. Liermann, S. Guha and U. Scherf, *Phys. Rev. E*, 2013, **87**, 022602.

11 a) P. A. Korevaar, C. Schaefer, T. F. A. de Greef and E. W. Meijer, *J. Am. Chem. Soc*., 2012, **134**, 13482; b) R. M. E. Marzal, P. C. Nalam, S. Bolisetty and N. D. Spencer, *Soft. Matter*, 2013, **9**, 4045; c) J. Mei, N. L. C. Leung, R. T. K. Kwok, J. W. Y. Lam and B. Z. Tang, *Chem. Rev.*, 2015, **21**, 11718; d) P. Jonkheijm, P. V. D. Schoot, A. P. H. J. Schenning and E. W. Meijer, *Science*, 2006, **313**, 80.

12 a) W. Y. So, J. Hong, J. J. Kim, G. A. Sherwood, K. Chacon-Madrid, J. H. Werner, A. P. Shreve, L. A. Peteanu and J. Wildeman, *J. Phys. Chem. B*, 2012, **116**, 10504. b) X. Wang, G. Guerin, H. Wang, Y. Wang, L. Manners and M. A. Winnik, *Science*, 2007, **317**, 644.

13 a) J. W. Steed and J. L. Atwood, *Supramolecular Chemistry*, 2nd Ed, Wiley (2013); b) Y. Kawanami, S. Y. Katsumata, J.-i. Mizoguchi, M. Nishijima, G. Fukuhara, C. Yang, T. Mori and Y. Inoue, *Org. Lett.*, 2012, **14**, 4962; c) N. Basilio, A. Pinetro, J. P. D. Silva and L. G. Rio, *J. Org. Chem.*, 2013, **78**, 9113.

14 J. Kumaki, T. Kawauchi, K. Okoshi, H. Kusanagi and E. Yashima, *Angew. Chem. Int. Ed.*, 2007, **46**, 5348.

15 a) J. J. van Gorp, J. A. J. M. Vekemans and E. W. Meijer, *J. Am. Chem. Soc.*, 2002, **124**, 14759; b) M. M. J. Smulders, I. A. W. Filot and E. W. Meijer, *J. Am. Chem. Soc*., 2010, **132**, 611; c) J. Tabei, R. Nakamura, F. Sanda and T. Masuda, *Macromolecules*, 2004, **37**, 1175; d) J. Tabei, R. Nakamura, F. Sanda and T. Masuda, *Macromolecules*, 2003, **36**, 8603.

16 a) M. M. Green, R. A. Gross, F. C Schilling, K. Zero and C. Crosby III, *Macromolecules*, 1988, **21**, 1839; b) D. Pijper, M. G. M. Jongejan, A. Meetsma and B. L. Feringa, *J. Am. Chem. Soc.,* 2008, **130**, 4541; c) T. Kajitani, H. Onouchi, S. I. Sakurai, K. Nagai, K. Okoshi, K. Onitsuka and E. Yashima, *J. Am. Chem. Soc*., 2011, **133**, 9156.

17 a) J. M. Lehn. *Angew. Chem. Int. Ed. Engl.*, 1990, **29**, 1304; b) C. R. Ray and J. S. Moore, *Adv. Polym. Sci.*, 2005, **177**, 91; c) Y. Nagata, T. Yamada, T. Adachi, Y. Akai, T. Yamamoto and M. Suginome, *J. Am. Chem. Soc*., 2013, **135**, 10104.

18 a) A. Harada and K. Kataoka. *Macromolecules*, 1995, **28**, 5294; b) A. Harada and K. Kataoka. *Science*, 1999, **283**, 65.

19 a) A. R. A. Palmans and E. W. Meijer. *Angew. Chem. Int. Ed. Engl.*, 2007, **46**, 8948; b) J. Kim, J. Lee, W. Y. Kim, H. Kim, S. Lee, H. C. Lee, Y. S. Lee, M. Seo and S. Y. Kim. *Nat. Commun*., 2015, **6**, 6959**.**

20 a) D. Danovich, S. Shaik, F. Neese, J. Echeverria, G. Aullon and S. Alvarez. *J. Chem. Theory Comput*., 2013, **9**, 1977; b) J. Echeverria, G. Aullon, D. Danovich, S. Shaik and S. Alvarez. *Nat. Chem*., 2011, **3**, 323; c) A. Michalak, M. Mitoraj and T. Ziegler, *J. Phys. Chem. A*, 2008, **112**, 1933.

21 a) S. K. Rajagopal, A. M. Philip, K. Nagarajan and M. Hariharan, *Chem. Commun*., 2014, **50**, 8644; b) K. Nagarajan, S. K. Rajagopal and M. Hariharan, *CrystEngComm*, 2014, **16**, 8946.

22 For recent reviews. a) T. Aida, E. W. Meijer and S. I. Stupp, *Science*, 2012, **335**, 813; b) T. F. A. de Greef and E. W. Meijer, *Nature*, 2008, **453**, 171; c) L. Yang, X. Tan, Z. Wang and X. Zhang, *Chem. Rev*., 2015, **115**, 7196; d) E. Krieg, M. M. C. Bastings, P. Besenius and B. Rybtchinski, *Chem. Rev*., 2016, **116**, 2414; e) M. Verswyvel and G. Koeckelberghs, *Polym. Chem*., 2012, **3**, 3203.